Mechanosynthesis of intermetallic $Fe_{100-x}Al_x$ obtained by reduction of Al/Fe_2O_3 composite

2000 J. Phys.: Condens. Matter 12 10579

(http://iopscience.iop.org/0953-8984/12/50/318)

J. Phys.: Condens. Matter **12** (2000) 10579–10590. Printed in the UK PII: S0953-8984(00)15463-3

Mechanosynthesis of intermetallic $Fe_{100-x}Al_x$ obtained by reduction of Al/Fe_2O_3 composite

G F Goya† and H R Rechenberg

Instituto de Física, Universidade de São Paulo, CP 66318, 05315-970 São Paulo, Brazil

E-mail: goya@macbeth.if.usp.br

Received 13 July 2000, in final form 23 October 2000

Abstract. Al_xFe_{100-x} alloy has been obtained through mechanical alloying of $Al + Fe_2O_3$ under an argon atmosphere. The resulting phase has a composition close to $Al_{30}Fe_{70}$ with disordered body-centred cubic structure and cell parameter $a = 2.892(4)$ Å. The magnetic properties studied by Mössbauer and magnetization measurements are consistent with an $x \sim 30$ composition. Annealing at 983 K produces only minor changes in the magnetic properties. A possible mechanism for formation of Al_xFe_{100-x} is suggested, consisting of (a) initial grain downsizing to nanometric scale and (b) subsequent decomposition of α-Fe_2O_3 producing metallic iron that is dissolved into the Al matrix. In contrast, no new phases were produced in a twin experiment on ball-milled $Fe + Al_2O_3$, carried out under identical milling conditions.

1. Introduction

Mechanical alloying (MA) is a widely used technique that allows the manufacturing of nanostructured powders. Ultrafine metallic powders are of importance in many applications including catalysis, magnetoresistive materials, and magnetic recording media. Recently, enhanced magnetoresistance has been observed in nanostructured metal–ceramic composites, which has been associated with spin-polarized tunnelling through spin-disordered particle surfaces [1, 2]. During mechanical alloying the particles are subjected to continuous cold welding and fracturing, yielding nanometric structures with clean surfaces at the atomic level. When these surfaces are brought into contact, new composite phases can be formed. A remarkable result of the MA dynamics is the formation of metastable phases even for systems with large negative mixing enthalpy. The ways in which these thermodynamic energy barriers are overcome are far from being understood. For example, in ball-milled Fe–Cu alloy, which is perhaps the most studied among these metastable systems, the thermodynamic and kinetic mechanisms that increase the solubility are still unknown [3, 4]. Mechanosynthesis of several oxides, sulphides, and other complex compounds has been successfully achieved by MA of the elemental powders [5–8]. These mechanochemical reactions offer the possibility of producing metastable nanostructures that cannot be obtained by other processes.

Disordered $Fe_{100-x}Al_x$ alloys have been produced by many different techniques [9–11] to study solubility ranges, amorphization mechanisms, and short- and long-range disorder that could improve their mechanical properties. In this system, it is known that plastic deformation produces structural disorder within the b.c.c. structure [12–14]. The increase in the number of antiphase boundaries (APB) yields magnetic order by enhancing the Fe–Fe magnetic

† Author to whom any correspondence should be addressed.

0953-8984/00/5010579+12$30.00

interactions, which turn the system ferromagnetic at room temperature for $x < 40$ [15]. Spin-glass-like (SGL) properties have also been observed at low temperatures for compositions in the $30 < x < 50$ range, although there is not yet clear evidence of magnetic frustration from ferromagnetic and antiferromagnetic interactions that could explain the SG state [16, 17]. Recently, an Ising model for disordered $Fe_{100-x}Al_x$ has been proposed, which predicts that the SGL state could originate from second-neighbour exchange interactions of Fe atoms for values of x in a specific range [18]. In this work, we have attempted to produce Al_xFe_{100-x} alloy by MA starting from Al/Fe_2O_3 composite, to study the structural disorder of the resulting phase, and its effects on magnetic properties. To investigate the chemical processes during mechanical alloying of Fe–Al–O systems, we performed a parallel experiment starting from Fe/Al_2O_3 and using identical milling conditions. Both sets of results are analysed and compared with previous data on Al–Fe alloys obtained by different methods.

2. Experiment

Samples of Al_xFe_{1-x} composite were prepared by mixing α-Fe_2O_3 (99.99% purity, 200 mesh) and metallic Al (99.99% purity, average particle size < 100 μm) with nominal composition $Al + Fe_2O_3$. The initial compounds were manually mixed in an agate mortar and afterwards introduced into the vials. To avoid oxidation of the metallic phase, the whole process of sample manipulation and vial sealing was done under an Ar atmosphere in a glove box (<12 ppm O_2, <12 ppm H_2O). The mixture was milled in a commercial planetary ball mill (Fritsch Pulverisette 7) for 365 h, using hardened steel vials and balls. The vials were kept closed during the entire milling process to prevent oxygen contamination. The ratio of ball/powder masses was chosen as 20:1, and the milling intensity set as 900 rpm. The milling operation was set to work on six-hour intervals (5 h on + 1 h off). The external temperature of the vials was measured after 100 hours of operation; we found a value $T = 378(5)$ K after a five-hour continuous working period. This value decreased to $T = 355(5)$ K during the one-hour rest interval. High pressure was detected inside the vials at the end of the whole process. Fractions of the resulting powder were subsequently heated at 783 K and 983 K for 2 h in an evacuated quartz tube at 10^{-5} Torr (labelled samples AF5 and AF7, respectively). In a twin experiment, a mixture of equimolar ratio $Fe:Al_2O_3$ was ball milled following the same procedure as described above (i.e. keeping the same milling time, masses, velocity, etc). In this case, no overpressure was observed after the process. A fraction of the resulting powder was annealed at 783 K (the same procedure as for AF5 sample).

X-ray diffraction patterns were obtained in a Philips PW-1140 diffractometer using Cu Kα radiation ($\lambda_{\alpha 1} = 1.540\,60$ Å). Magnetization versus applied field measurements were performed in a VSM magnetometer, between 4 K and 300 K, in external fields up to 90 kOe. Alternating- and direct-current magnetization versus temperature curves were measured in a commercial SQUID magnetometer in the $5\ \text{K} < T < 400$ K range. The frequency of the a.c. driving field was $f = 133.3$ Hz, and the amplitudes were from 3 to 50 Oe. Mössbauer spectra were taken at 4.2, 80, and 300 K in the transmission geometry, using a ^{57}Co source in constant-acceleration mode. Hyperfine-field distributions, with Lorentzian lineshapes, were used to fit the spectra. Isomer shifts are referred to α-Fe at 300 K.

3. Results

Figure 1 shows the x-ray diffraction (XRD) patterns for the as-milled sample. The Rietveld method was used to determine the structural parameters [19]. The observed peaks were indexed

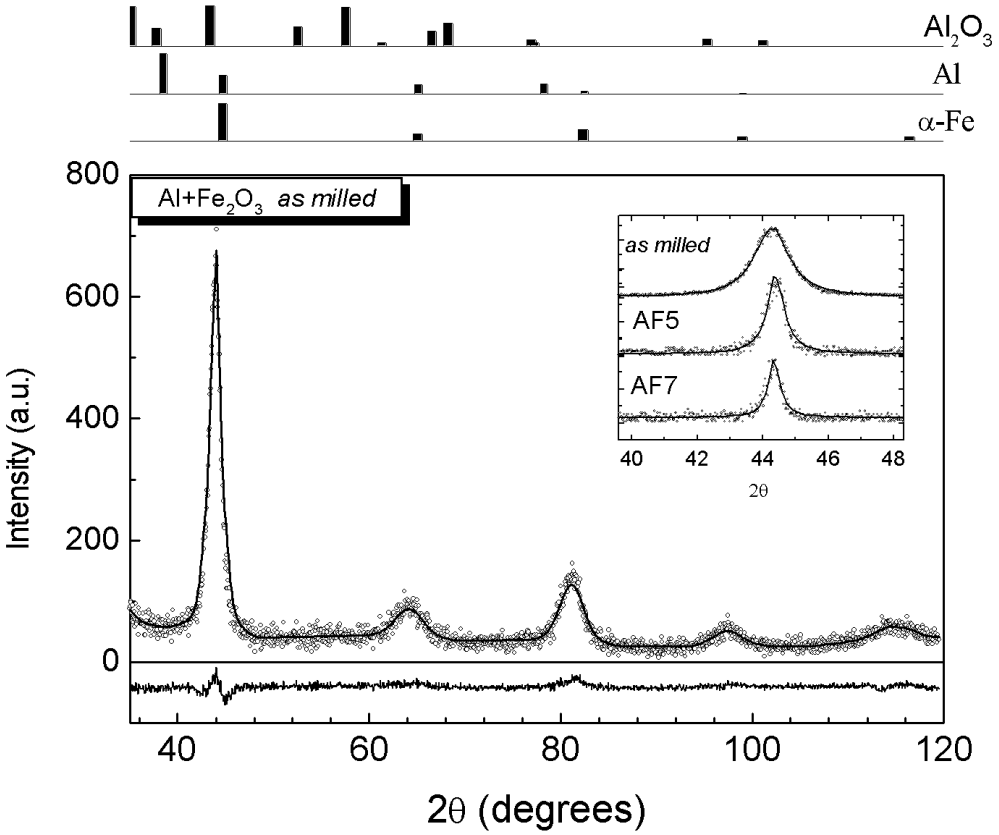

Figure 1. The observed and calculated x-ray powder diffraction pattern and difference plot for the as-milled sample. Inset: the evolution of the 110 peak after annealing at 783 K (sample AF5) and 983 K (sample AF7). The lines expected for α-Fe, Al, and Al_2O_3 are also indicated (reference [40]).

as AlFe phase with b.c.c. structure and lattice parameter $a = 2.892(4)$ Å. The broad peaks are expected from the small domain sizes and high microstrain resulting from the milling process. No other peaks were observed within the experimental resolution. The average grain diameter $\langle d \rangle$ estimated from the 110 peak, using Scherrer's equation, was $\langle d \rangle = 7(3)$ nm. For annealed samples AF5 and AF7 this value increases to $\langle d \rangle = 14(3)$ and 20(3) nm, respectively (see the inset of figure 1). However, the above estimates must be taken as rough approximations, since ball-milled Al–Fe alloy is known to be composed of a mixture of disordered b.c.c. and ordered B2 phases which contribute to the XRD linewidth, and hence a precise deconvolution of both lines is needed [20]. Superstructure reflections from the chemical order of the Fe and Al atoms ($j + k + l$ odd) were absent, in agreement with the disordered nature of the resulting phase. No other phases were detected, within experimental error, from the XRD patterns of as-milled, AF5, or AF7 samples. This fact, also supported by Mössbauer data (discussed below), suggests nearly complete reaction of the starting Al/Fe_2O_3 mixture.

Room temperature Mössbauer spectra of as-milled and annealed samples are shown in figure 2. The three spectra show similar hyperfine-field distributions, spanning from $B_{hf} \sim 17$ to 34 T. The maximum of the distribution is located at $B_{hf} = 28.9(3)$ T for the as-milled sample, in agreement with previous data on disordered $Fe_{100-x}Al_x$ samples with $x \sim 30$ obtained by different methods [9, 15, 21]. Mössbauer spectra taken at 4.2 K (figure 3) show

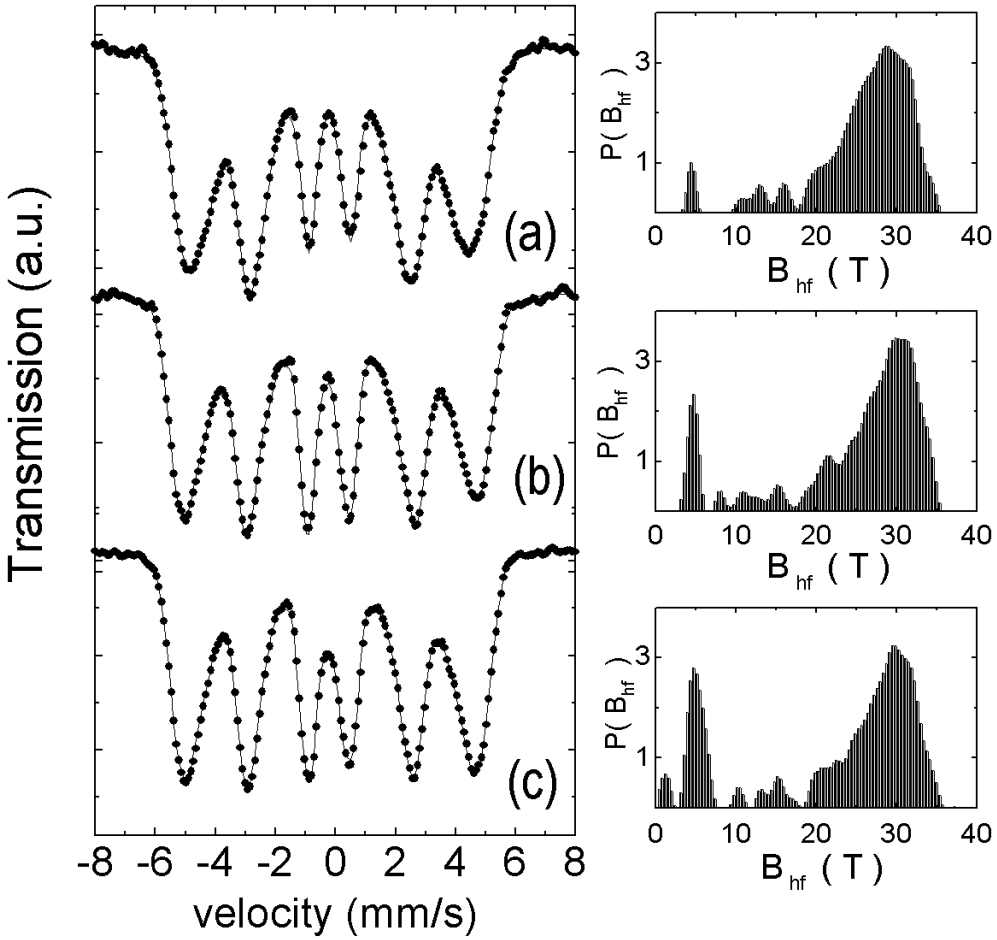

Figure 2. Room temperature Mössbauer spectra of (a) as-milled, (b) AF5, and (c) AF7 samples. The corresponding hyperfine-field distributions are shown on the right-hand side.

similar hyperfine-field distributions, without any signs of further magnetic ordering. For annealed AF5 and AF7 samples, the hyperfine-field distributions are slightly narrower and show coincident maxima at $B_{hf} = 32.0(3)$ T. From the hyperfine-field distributions at room temperature, one can observe the appearance of a small peak at $B_{hf} = 5$ T, which increases upon annealing the samples. We assign this peak to Fe sites with increased numbers of Al first and second neighbours, leading to lower hyperfine fields. These regions of weak Fe–Fe interactions could order at lower temperatures, explaining the disappearance of this peak for $T = 4.2$ K.

Magnetization versus applied field curves recorded at $T = 4.2$ K display full magnetic saturation for fields $H > 20$ kOe, and low coercivity $H_C \sim 50$ Oe (see table 1) for as-milled and annealed samples, which remain nearly unchanged within the 300–4.2 K range. The value of the coercive field did not show any dependence on the cooling process; i.e. ZFC or FC with $H_{FC} = 90$ kOe procedures yielded the same H_C-values. The saturation magnetization at room temperature for the as-milled sample, $M_S = 162.2(5)$ emu g^{-1}, is very close to previously reported results for disordered Al_xFe_{100-x} alloys with $x = 30$ [21]. Magnetization curves of

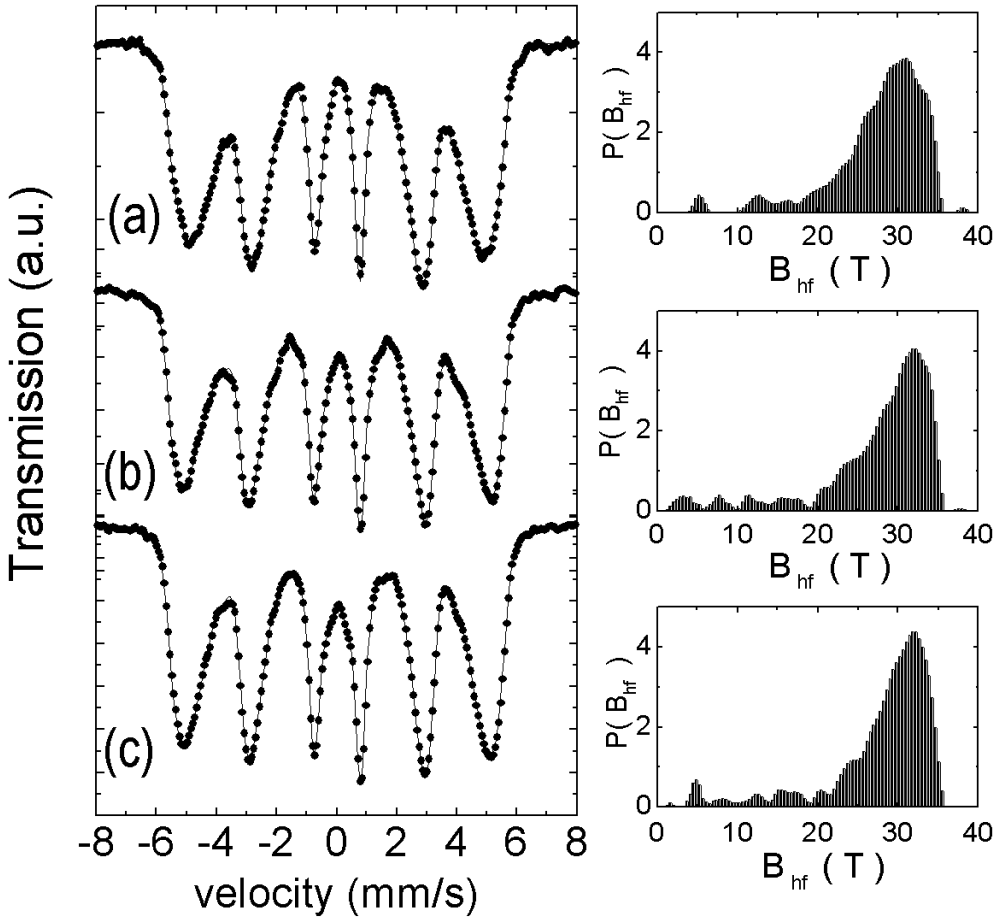

Figure 3. Mössbauer spectra at $T = 4.2$ K of (a) as-milled, (b) AF5, and (c) AF7 samples. The corresponding hyperfine-field distributions are shown on the right-hand side.

Table 1. Saturation magnetization (M_S), coercivity (H_C), and remanence (M_R) of as-milled and AF7 samples, at 4.2 K and room temperature.

T (K)	Sample	M_S (emu g^{-1})	H_C (Oe)	M_R (emu g^{-1})
4.2	As milled	163.0(5)	61(2)	4.4(8)
	AF7	153.6(5)	59(2)	2.6(8)
300	As milled	162.2(5)	54(2)	3.4(8)
	AF7	153.2(4)	53(2)	2.2(8)

as-milled and AF7 samples recorded in ZFC and FC modes with an applied field $H_{FC} = 3$ Oe are shown in figure 4. The ZFC branch for the as-milled sample increases with increasing temperature showing no definite peaks associated with spin-glass or superparamagnetic ordering. For the annealed AF7 sample, a broad peak develops at $T \sim 300$ K. The increase in both FC branches shows that the samples are not fully ordered after field cooling with a small field $H_{FC} = 3$ Oe. However, monotonically decreasing behaviour is observed in the FC branches when $H_{FC} = 50$ Oe is applied (figure 5), indicating that the anisotropy fields in

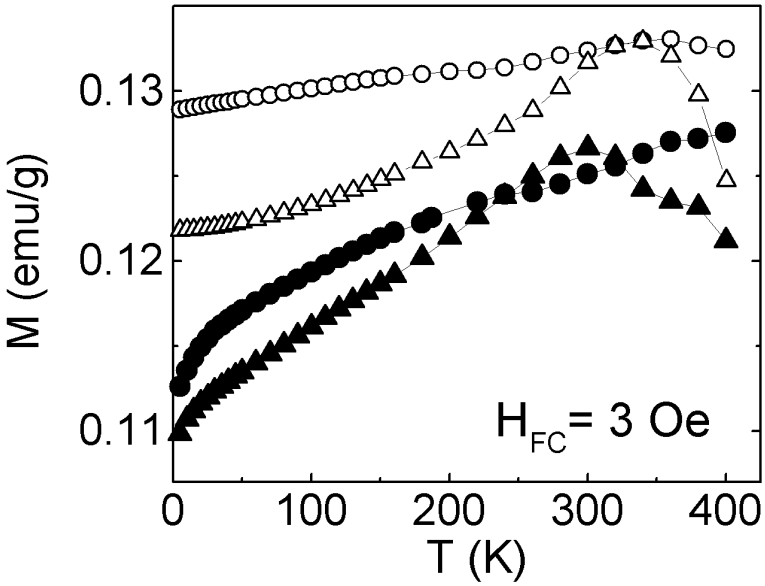

Figure 4. Magnetization curves of as-milled (circles) and AF7 (triangles) samples measured with $H_{FC} = 3$ Oe. Filled symbols correspond to the zero-field-cooling mode and open symbols to the field-cooling mode.

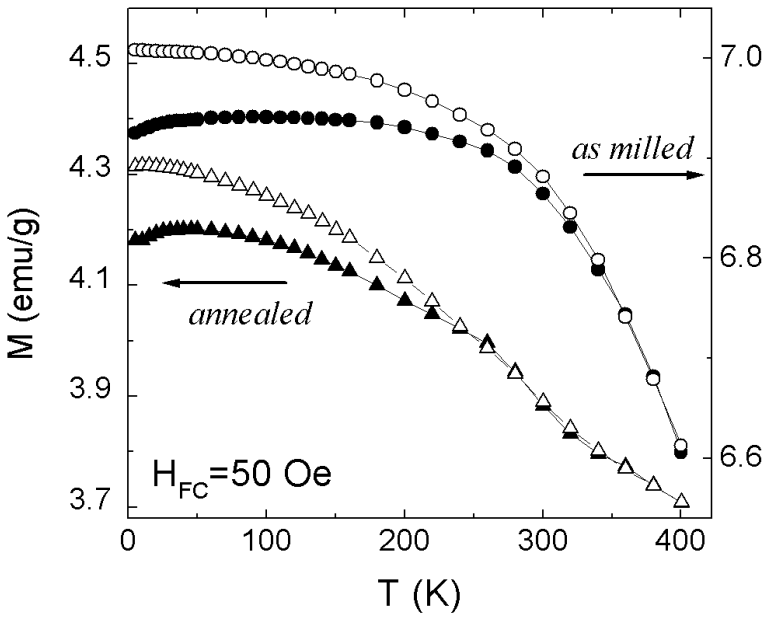

Figure 5. Magnetization curves of as-milled (circles) and AF7 (triangles) samples measured with $H_{FC} = 50$ Oe. Filled symbols correspond to the zero-field-cooling mode and open symbols to the field-cooling mode.

these samples are of about this magnitude. This is in agreement with the measured values of $H_C \sim 50$ Oe for all samples (see table 1). In addition, the irreversibility observed in ZFC–FC

branches, which extends beyond $T = 400$ K for $H_{FC} = 3$ Oe, shifts down to the $T \sim 250$ to 300 K range for $H_{FC} = 50$ Oe. The in-phase (χ') component of the a.c. susceptibility, for both samples (figure 6), decreases for $T > 300$ K. Extrapolation of both $\chi'(T)$ curves (assuming monotonic behaviour) for $T > 400$ K gives $\chi' = 0$ at $T \sim 600(20)$ K, suggesting that the ferromagnetic-to-paramagnetic transition could be located at this temperature. Relaxation mechanisms can be discarded since no change in the out-of-phase component is observed in this temperature range (see figure 6). The series of three peaks observed at $T = 13$, 64, and 120 K might be associated with relaxation of domains with different energy barriers.

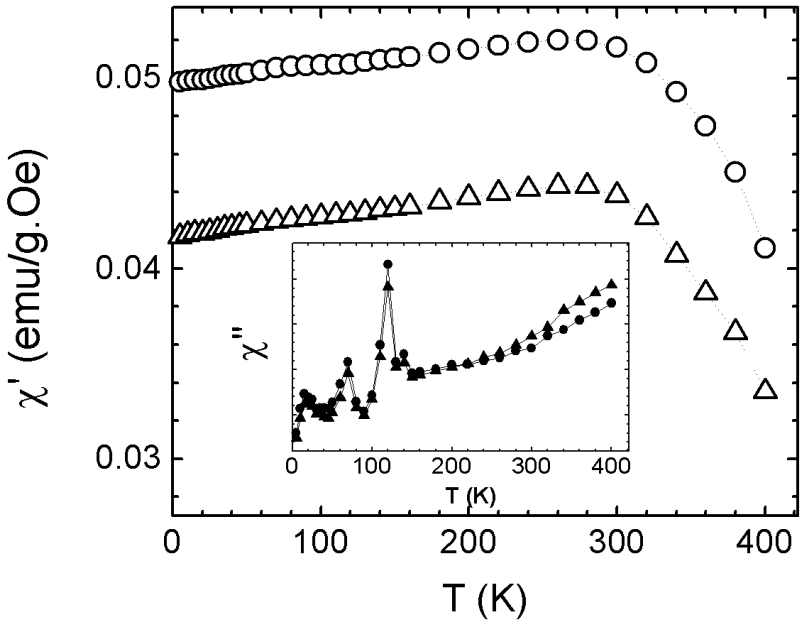

Figure 6. In-phase components of the a.c. susceptibility for as-milled (circles) and AF7 (triangles) samples, measured after zero-field cooling. The inset shows the corresponding out-of-phase components.

With the aim of further investigating the evolution of Fe–Al phases during mechanical alloying, a mixture of Fe + Al_2O_3 was subjected to the same conditions of MA as the previous sample Al/Fe_2O_3. In this case, the XRD data showed no change in the initial composition after 365 h of milling. The most intense lines were indexed as b.c.c. iron, and weak peaks corresponding to Al_2O_3 were detected. The difference between the intensity of the Fe and Al_2O_3 lines suggests smaller particle size and/or higher degree of amorphization of the latter. Evidence of unreacted Fe was also found in Mössbauer spectra at room temperature (figure 7), which show the characteristic magnetically split sextet of b.c.c. iron, with a hyperfine field $B_{hf} = 33.0$ T. A central doublet amounting to ∼4% of the total resonant area was also observed, which disappears upon annealing the sample at 783 K in vacuum. The hyperfine parameters $\Delta Q = 0.87(3)$ mm s^{-1} and IS $= 0.33(1)$ mm s^{-1} of this doublet are typical of those observed for various Fe oxide superparamagnetic particles, suggesting that some oxidation could have occurred during milling. The as-milled sample displays soft magnetic properties expected for metallic Fe. It can be observed from the ZFC–FC data (figure 8) that even a small external field of $H_{FC} = 10$ Oe completely saturates the magnetization after field cooling (compare with figures 4 and 5). The steady increase of the ZFC branch indicates a

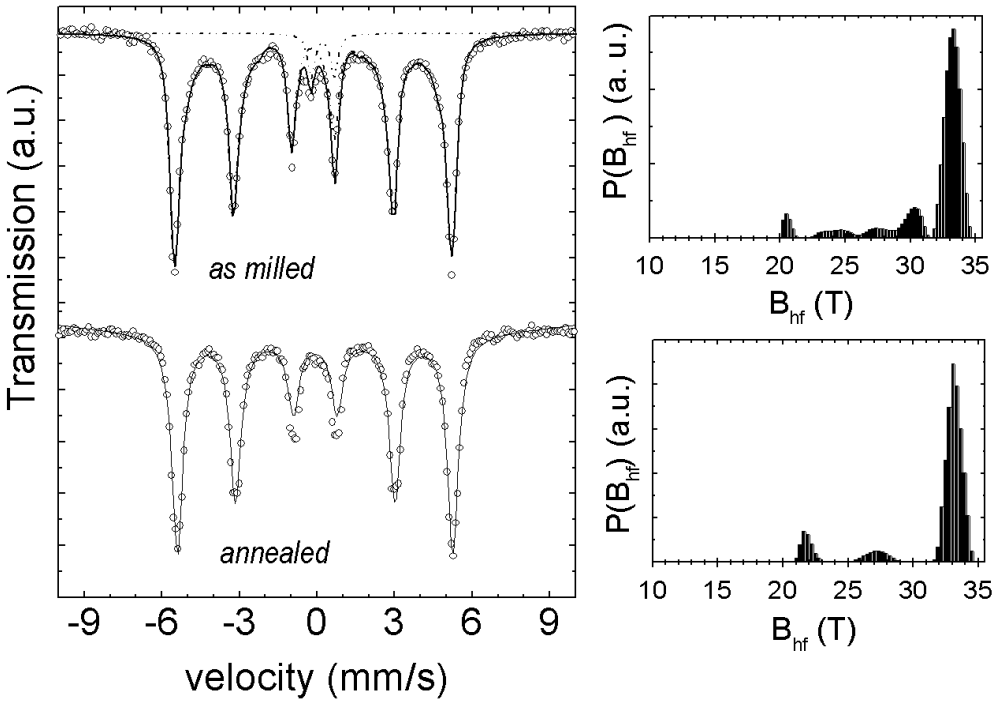

Figure 7. Room temperature Mössbauer spectra of the Fe + Al_2O_3 sample (a) as-milled and (b) annealed at 783 K. The corresponding hyperfine-field distributions are shown on the right-hand side.

broad distribution of particle sizes. Assuming that the starting Fe/Al_2O_3 composition did not change during milling, the calculated saturation magnetization at $T = 300$ K of the as-milled sample is $M_S = 207$ emu g(Fe)$^{-1}$, close to the theoretical 217.2 emu g^{-1} value for pure b.c.c. iron (see the inset of figure 8). The above data indicate that most of the starting Fe and Al_2O_3 phases did not react during milling, under the same conditions as were used for the Al/Fe_2O_3 mixture.

4. Discussion

Chemical reduction of different transition metals induced by MA has been previously accomplished in many systems, by using strongly reducing elements such as C, Ca, and Na over the corresponding metal chloride or oxide [6, 22–24]. These reducing elements are usually chosen to ensure a large enthalpy of formation (about 10^2–10^3 kJ mol^{-1}) which favours the displacement reactions from reactants to final products.

It is well known [25] that haematite (α-Fe_2O_3) can be transformed into magnetite (Fe_3O_4) by high-energy ball milling in a closed container and, furthermore, that subsequent milling in air [26] can reverse this reaction. One of the explanations proposed for this reaction [25, 26] involves breaking of the α-Fe_2O_3 chemical bonds and thus oxygen release during ball milling. The suggested mechanism is related to the concept of mechanosynthesis, where chemical bonds are necessarily broken in order to sustain a solid-state reaction. Several works on the reduction of α-Fe_2O_3 and Fe_3O_4 by aluminium have been previously reported [27–29]. In the work of Concas *et al* [28], reduction of haematite by aluminium in an argon atmosphere was

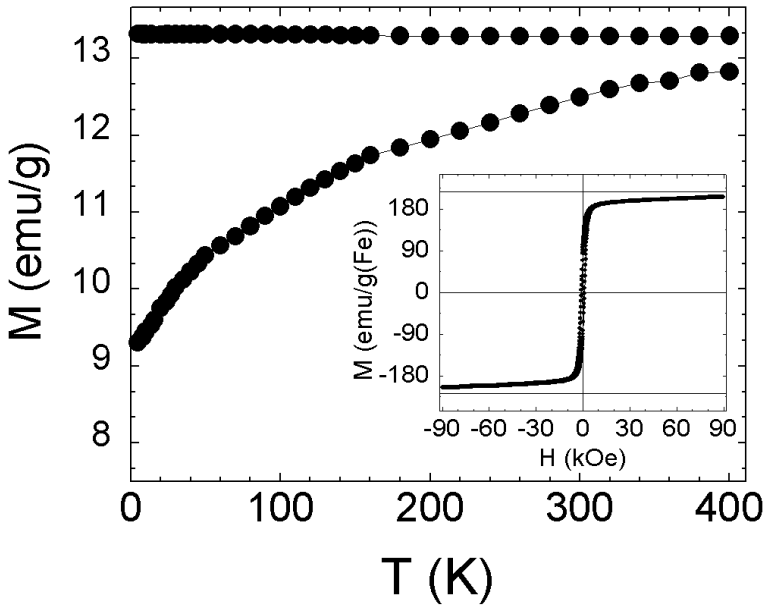

Figure 8. ZFC–FC curves of the as-milled Fe + Al_2O_3 sample with $H_{FC} = 10$ Oe. Inset: the M versus H curve taken at $T = 300$ K. The horizontal full lines indicate the saturation values for pure Fe.

reported, yielding a mixture of α-Fe, Fe–Al alloy, and $FeAl_2O_4$ phases. However, their use of Al_2O_3 as the diluent prevents a direct comparison with our results.

Although intermediate phases containing Fe^{2+} such as magnetite or hercynite might be formed during the reduction process, the absence of Fe^{2+} in Mössbauer spectra (easily detectable from its distinctive hyperfine parameters) can be explained by the long milling time. For the study of phase evolution, several samples with intermediate milling times would be needed. It is worth noting that this should be done by several independent milling experiments, since stopping the milling to extract partial amounts of the sample would modify the pressure and composition of the atmosphere inside the vials.

In a recent paper [30] on mechanically driven reduction of CuO by Al, it was found that the initial CuO is gradually reduced by Al, resulting in metastable Al_4Cu_9 alloy. With their starting compositions Al–5CuO and Al–10CuO and assuming complete reaction of all of the (less abundant) Al available, the redox balance of the reaction $CuO + Al \rightarrow Cu + Al_2O_3$ gives a final ratio $Al_2O_3/Cu \sim 0.5$, while a significant fraction of the starting CuO should remain unreacted. However, the XRD patterns showed no evidence of Al_2O_3. The authors assigned this feature to a low amount of Al_2O_3 formed and its possible amorphization. Similarly, in the work of Xi Shengqi *et al* [31] on ball-milled CuO/Al, the relative amount of Al_2O_3 inferred from XRD data is clearly lower than the 0.5 value.

In the present experiment, if a similar mechanism for partial reduction of Fe_2O_3 by all of the initial Al is assumed, the reaction could be represented by

$$2Al^0 + 2Fe_2O_3 \rightarrow 2Fe^0 + Al_2O_3 + Fe_2O_3 \qquad \text{(I)}$$

yielding 27 and 42 wt% of Al_2O_3 and Fe_2O_3 phases as final products, respectively. The presence of haematite or other iron-containing oxides after milling can be discarded from Mössbauer spectra within the experimental error (about 1% of the resonant area of Fe compounds). On

the other hand, the absence of the corresponding peaks in the XRD patterns (see figure 1) implies that, if reaction (I) takes place, the resulting Al_2O_3 and Fe_2O_3 must be completely amorphized. In view of the extended milling time of our experiment, we have also examined the possibility of reaction (I) being an intermediate stage of the phase evolution. However, comparison with previous experiments on Al/Fe_3O_4 [29], Fe/Fe_3O_4 [32], and Fe/Al_2O_3 [33] shows that the final powder should contain FeO, α-Fe_2O_3, Fe_3O_4, or $FeAl_2O_4$ phases, which are not found in Mössbauer spectra. From the above results, it seems unlikely that reaction (I) is the main mechanism for chemical reduction of Fe^{3+} during ball milling.

In the ball-milled samples, the structural and magnetic properties evolve as a function of milling time, attaining 'saturation' values asymptotically for long enough times [12, 20, 34]. Although it is not possible to compare timescales between different milling experiments, there is an acceptable consistency between the magnetic and structural data for different samples of milled Al–Fe, provided that this 'saturation' regime is reached [14, 21]. In particular, the cell volume and hyperfine fields for $Fe_{100-x}Al_x$ seem to be definite functions of x, not only for crystalline samples but also for disordered samples.

Our XRD pattern of the as-milled sample was indexed with the $Fe_{100-x}Al_x$ b.c.c. phase, having a cell parameter, a, about 1% higher than the corresponding one for pure b.c.c. iron. This is consistent with the increase of the unit-cell volume of the FeAl alloy with higher Al contents [15, 35–37]. Since it was not possible to extract a precise value of x from x-ray data refinement, the Al composition was estimated by comparison with the systematic determinations of the lattice parameter in Al–Fe alloys of references [15] and [35]. These works show similar evolution of a with Al content, in spite of their different preparation methods and milling times. The interpolation of our a-value, for both curves, yields values of x between 20 and 30 at.%, close to the Al:Fe atomic ratio of the initial mixture.

Regarding the magnetic properties of $Fe_{100-x}Al_x$ alloys, many works have demonstrated that ferromagnetic order appears for $x < 33$, but this range can be extended up to $x \sim 65$ through mechanical alloying or plastic deformation [14, 15, 38, 39]. It is interesting to note that Mössbauer spectra and hyperfine-field distributions of the as-milled sample in figures 2 and 3 are very similar to the data reported by other authors [9, 15, 21, 36] for $x = 30$. The abrupt change in the shape of the spectra around the $x = 30$ composition also supports this comparison†. Regarding magnetization values, we are not aware of previous measurements on milled $Fe_{100-x}Al_x$ samples as functions of x. However, the work of Jartych *et al* [21] on milled $Fe_{70}Al_{30}$ showed that M increases with milling time, attaining a value $M(T) \sim 150$ emu g^{-1} at room temperature for $t = 100$ h, and remains essentially constant for longer milling times. Accordingly, the value for our as-milled sample is $M_S(4.2\ \mathrm{K}) = 163.0(5)$ emu g^{-1}, and slightly decreases with reordering (i.e. upon annealing the sample) to 153.6(5) emu g^{-1}.

On the basis of the above reasoning, we proposed a different mechanism to account for the formation of the resulting phase:

$$\mathrm{Al} + \mathrm{Fe_2O_3} \rightarrow 3\mathrm{Fe_{0.67}Al_{0.33}} + 1.5\mathrm{O_2} \uparrow \qquad \text{(II)}$$

which has the redox balance needed to explain the chemical reaction within the closed vials during milling, through which the Al_xFe_{100-x} alloy is formed. The released oxygen could also explain the overpressure found inside the vials after milling. From the redox balance and the increase of temperature measured, the pressure inside the vials during reaction (II) should attain a value of about 3 atm. However, incomplete sealing of the vials might result in lower values. To measure the amount of oxygen released, further experiments measuring temperature and pressure inside the vials during milling are currently under way.

† Compare, for example, the as-milled spectra (figure 2) with figure 2 of Eelman *et al* (reference [15]) and figure 3 of Enzo *et al* (reference [36]).

In reaction (II) the Al atoms appear to act as a catalytic agent for decomposition of Fe_2O_3. Regarding phase evolution, it seems conceivable that the initial particle size reduction to the nanometre scale provides the conditions for reduction of Fe^{3+} to metallic Fe, and further dispersion into the Al matrix. The fact that the milled Fe/Al_2O_3 mixture does not show phase reactions suggests that redox potentials of the $Fe/Al^{3+} \leftrightarrow Al/Fe^{3+}$ reactions could govern the process. However, the detailed mechanisms by which reaction (II) takes place are still to be determined.

In summary, we have produced nanostructured b.c.c. $Fe_{100-x}Al_x$ ($x \sim 30$) alloy by mechanochemical reaction starting from the Al/Fe_2O_3 composite. XRD, Mössbauer, and magnetization measurements indicate that the resulting alloy originates from reduction of the Fe_2O_3 to Fe and subsequent reaction to form $Al_{30}Fe_{70}$.

Acknowledgment

This work was supported by the Fundação de Amparo à Pesquisa do Estado de São Paulo (FAPESP).

References

[1] Ziese M 1999 *Phys. Rev.* B **60** R738
[2] Zhu T and Wang Y J 1999 *Phys. Rev.* B **60** 11 918
[3] Huang J Y, Jiang J Z, Yasuda H and Mori H 1998 *Phys. Rev.* B **58** R11 817
[4] Ma E and Atzmon M 1995 *Mater. Chem. Phys.* **39** 249
[5] Tsuzuki T and McCormick P G 1999 *Nanostruct. Mater.* **12** 75
[6] Schaffer G B and McCormick P G 1989 *Appl. Phys. Lett.* **55** 45
[7] Goya G F and Rechenberg H R 1999 *J. Magn. Magn. Mater.* **203** 141
[8] Eckert J, Schultz L and Urban K 1989 *Appl. Phys. Lett.* **55** 117
[9] Takahashi S, Onodera H, Li X G and Miura S 1997 *J. Phys.: Condens. Matter* **9** 9235
[10] Jaouen C, Rivière J P and Delafond J 1987 *J. Nucl. Instrum.* B **19–20** 554
[11] Liu H and Mitchell T E 1983 *Acta Metall.* **31** 863
[12] Meyer M, Mendoza-Zelis L, Sánchez F H, Clavaguera-Mora M T and Clavaguera N 1999 *Phys. Rev.* B **60** 3206
[13] Bogner J, Steiner W, Reissner M, Mohn P, Blaha P, Schwarz K, Klachler R, Ipser H and Sepiol B 1998 *Phys. Rev.* B **58** 14 922
[14] Hernando A, Amils X, Nogués J, Suriñach S, Baró M D and Ibarra M R 1998 *Phys. Rev.* B **58** 11 864
[15] Eelman D A, Dahn J R, MacKay G R and Dunlap R A 1998 *J. Alloys Compounds* **266** 234
[16] Schukla P and Wortis M 1980 *Phys. Rev.* B **21** 159
[17] Grest G S 1980 *Phys. Rev.* B **21** 165
[18] Plascak J A, Zamora L E and Pérez Alcázar G A 2000 *Phys. Rev.* B **61** 3188
[19] Young R A (ed) 1995 *The Rietveld Method* (New York: Oxford University Press)
[20] Negri D, Yavari A R and Deriu A 1999 *Acta Mater.* **47** 4545
[21] Jartych E, Zurawicz J K, Oleszak D, Pekala M, Sarzynski J and Budzynski M 1998 *J. Magn. Magn. Mater.* **186** 299
[22] Mateazzi P and Le Caer G 1991 *Mater. Sci. Eng.* A **149** 135
[23] Forrester J S and Schaffer G B 1995 *Metall. Mater. Trans.* A **26** 725
[24] Ding J, Miao W F, McCormick P G and Street R 1995 *Appl. Phys. Lett.* **67** 3804
[25] Kaczmarek W A and Ninham B W 1994 *IEEE Trans. Magn.* **30** 732
[26] Linderoth S, Jiang J Z and Mørup S 1997 *Mater. Sci. Forum* **235–238** 205
[27] Cao G, Concas G, Corrias A, Orru R, Paschina G, Simoncini B and Spano G 1997 *Z. Naturf.* a **52** 539
[28] Concas G, Corrias A, Manca E, Paschina G and Spano G 1998 *Z. Naturf.* a **53** 239
[29] Takacs L 1992 *Mater. Lett.* **13** 119
[30] Wu J M and Li Z Z 2000 *J. Alloys Compounds* **299** 9
[31] Xi Shengqi, Qu Xiaoyan, Ma Mingliang, Zhou Jingen, Zheng Xiulin and Wang Xiaotian 1998 *J. Alloys Compounds* **268** 211
[32] Ding J, Miao W F, Pirault E, Street R and McCormick P G 1998 *J. Magn. Magn. Mater.* **177–181** 933

[33] Linderoth S and Pedersen M S 1994 *J. Appl. Phys.* **75** 5867
[34] Gialanella S, Amils X, Baró M D, Delcroix P, Le Caer G, Lutterotti L and Suriñach S 1998 *Acta Mater.* **46** 3305
[35] Yelsukov E P, Voronina E V and Barinov V A 1992 *J. Magn. Magn. Mater.* **115** 271
[36] Enzo S, Frattini R, Gupta R, Macri P P, Principi G, Schiffini L and Scipione G 1996 *Acta Mater.* **44** 3105
[37] Sumiyama K, Hirose Y and Nakamura Y 1990 *J. Phys. Soc. Japan* **59** 2963
[38] Takahashi S, Li X G and Chiba A 1996 *J. Phys.: Condens. Matter* **8** 11 243
[39] de Toro J A, López de la Torre M A, Sáez Puche R and Rivero J M 1999 *J. Magn. Magn. Mater.* **196** 243
[40] Joint Committee on Powder Diffraction Standards (JCPDS) 1995 *Powder Diffraction Data Cards* No 06-0696, No 04-0787 and No 43-1484 (International Center for Diffraction Data)